Controlled nanocrystallinity in Gd nanobowls leads to magnetization of 226 emu/g

Y. N. Ertas and L.-S. Bouchard

Citation: Journal of Applied Physics **121**, 093902 (2017); doi: 10.1063/1.4977511
View online: http://dx.doi.org/10.1063/1.4977511
View Table of Contents: http://aip.scitation.org/toc/jap/121/9
Published by the American Institute of Physics

Controlled nanocrystallinity in Gd nanobowls leads to magnetization of 226 emu/g

Y. N. Ertas[1] and L.-S. Bouchard[1,2,3,a)]
[1]*Department of Bioengineering, University of California–Los Angeles, 420 Westwood Plaza, Los Angeles, California 90095, USA*
[2]*Department of Chemistry and Biochemistry, University of California–Los Angeles, 607 Charles E. Young Drive East, Los Angeles, California 90095, USA*
[3]*California NanoSystems Institute–UCLA, 570 Westwood Plaza, Los Angeles, California 90095, USA*

(Received 2 November 2016; accepted 14 February 2017; published online 1 March 2017)

Gadolinium (Gd) metal is of great interest in applications such as contrast-enhanced MRI and magnetic cooling. However, it is generally difficult to produce oxide-free and highly magnetic Gd nanoparticles due to the aggressively reactive nature of Gd with oxygen. Herein, we utilized a nanofabrication route and optimization of experimental conditions to produce highly magnetic air-stable oxide-free Gd nanoparticles. The nanobowls displayed the highest saturation magnetization to date for Gd, reaching 226.4 emu/g at 2 K. The crystalline composition of Gd is found to affect the observed magnetization values: the higher magnetization is observed for nanoparticles that have a lower content of the paramagnetic face-centered cubic (fcc) phase and a greater content of the ferromagnetic hexagonal close-packed (hcp) phase. The relative fcc content was found to depend on the deposition rate of the Gd metal during the nanofabrication process, thereby correlating with altered magnetization. *Published by AIP Publishing.*
[http://dx.doi.org/10.1063/1.4977511]

I. INTRODUCTION

Due to its unique high magnetic moment (268 emu/g at cryogenic temperatures) and high Curie temperature (293 K), Gd metal has been the subject of considerable interest over the past decade.[1] The magnetism of Gd arises from the presence of seven unpaired 4*f* electrons and magnetocrystalline anisotropy.[2] The magnetic properties of Gd display different characteristics than the standard ferromagnetic 3*d* metals such as Fe and Co.[2] Contrary to non-localized spins in 3*d* metals, 4*f* spins are indirectly coupled via the Ruderman-Kittel-Kasuya-Yosida interaction and strongly localized,[3] which brings unique magnetic behavior to Gd at the nanoscale. In recent years, Gd nanoparticles have found uses in magnetocaloric refrigeration,[4] neutron-capture therapy,[5] temperature sensing,[6] and MRI.[7] Previous studies investigated the fabrication and characterization of thin films,[8] multilayers,[9] and nanostructures[10–13] of Gd. In more recent work,[7] oxide-free Gd nanoparticles have been developed. Until this work, the primary chemical synthesis methods for Gd resulted in the formation of oxides due to the aggressively reactive nature of Gd towards oxygen in ambient air. The applications and uses of Gd have thus been drastically hampered, thereby limiting our ability to probe the physical and material properties of Gd in nanoparticle form. The magnetization of Gd thin films is notably different from that of bulk crystals due to the granular structure, size, and shape-related effects.[1] Nanoparticles of Gd are also expected to possess different magnetic properties than the thin films.[14] Therefore, there is a need to produce oxide-free Gd nanoparticles and study their physical properties in nanoparticle form.

Several techniques[13,15–18] have been developed and applied to obtain nanoparticles and nanoscale powders of Gd, including alkalide reduction, gas-phase, arc-discharge, as well as the use of multilayer precursors. Such nanoparticles were not stable in ambient air, resulting in oxides of Gd. However, oxides of Gd possess inferior magnetic properties, making them unsuitable for studies of Gd in nanoparticle form.[19] We have recently proposed a novel approach based on a nanofabrication process to produce oxide-free stable Gd nanoparticles whereby a core-shell Gd nanoparticle structure is obtained.[7] The Gd core is grown by deposition of the Gd metal under high vacuum conditions whereas the shell layer provides the appropriate capping of the core, preventing oxidation. While this process managed to achieve the highest magnetizations for Gd nanoparticles to date, further optimization of the experimental conditions is possible.

To put our work in context, Table I compares the magnetization of our nanobowls to those of other Gd nanostructures and thin films previously published in the literature. The first general observation is that nanoparticles of Gd generally yield low magnetization values, whereas thin films are closer to bulk values. This is likely a consequence of greater surface effects in nanoparticles. Our nanoparticles exhibit magnetization values that are much closer to the bulk value of Gd compared to other nanoparticle synthesis methods. This is likely due to the oxide-free nature of our fabrication process.[7] In a previous study, it has been claimed that chemical synthesis could achieve oxide-free Gd nanoparticles.[21] However, these nanoparticles may not be exactly oxide-free, as evidenced by the larger magnetizations obtained here via our nanofabrication approach. When constructing this table, we have converted reported magnetization values to emu/g units to enable direct comparison, using the textbook density

a)Electronic mail: bouchard@chem.ucla.edu

TABLE I. Comparison of magnetization values for Gd nanostructures and thin films obtained in previous studies.

Reference #	Type of Gd structure	Magnetization, as reported	Magnetization in emu/g
This study	Nanoparticle	226.4 emu/g	226.4 emu/g
1	Thin film	2.6 T	261.9 emu/g
9	Thin film	1900 emu/cm^3	240.5 emu/g
19	Nanorod	460 emu/cm^3	58.2 emu/g
20	Bulk	268.4 emu/g	268.4 emu/g
21	Nanoparticle	156 emu/g	156 emu/g
27	Thin film	640 emu/cm^3	81 emu/g

value of 7.90 g/cm^3 for gadolinium and the unit conversion factor $1\,\mathrm{T} = 4\pi \times 10^{-4}$ emu/cm^3.

The main conclusion of this study is the report of the highest saturation magnetization (226.4 emu/g at 2 K) for Gd nanoparticles observed to date. This was obtained through the selection of the deposition rate during the nanofabrication process. The deposition rate of the Gd metal resulted in different relative compositions of fcc to hcp phases within the construct. This, in turn, correlated with the magnetic properties. The deposition rate during e-beam evaporation may offer a control parameter for nanoparticle properties.

II. EXPERIMENTAL

The nanoparticles were prepared using a nanolithography fabrication process whereby monolayers of polystyrene nanospheres are used as a templating pattern for material deposition. Two-inch *p*-type⟨100⟩ silicon wafers were spin-coated with a monolayer of polystyrene nanobeads of 200 nm diameter (PS200 NM Magsphere Inc., CA). The nanosphere solution was diluted with 1:1 (v/v) methanol solution to facilitate the spreading of the nanospheres on the wafer substrates for a more uniform coating and higher surface coverage. Wafers were also treated by O_2 plasma for 1 min with a plasma power of 100 W and O_2 flow of 50 sccm before the nanobead coating step to render the wafer surface hydrophilic, enabling the nanosphere solution to better disperse on the surface. Untreated wafers were found to have limited nanobead coverage with multilayer regions after the coating process. Oxygen reactive ion etching (RIE) was performed to reduce the size of the polymer nanospheres. By adjusting the duration and/or plasma power of this step, specific nanosphere sizes could be achieved. However, prolonged etching should be avoided as it eventually results in a loss of spherical shape. Process parameters were adjusted to obtain ~100 nm size spheres with proper spherical shapes, as verified by scanning electron microscopy (SEM). Layers of 10 nm of SiO_2, 10 nm of Gd of 99.95% purity, and 20 nm of SiO_2 layers were, respectively, deposited by electron-beam evaporation onto the 15° tilted substrates under high vacuum ($<10^{-6}$ mtorr) to create Gd@SiO_2 layers onto the etched nanospheres. During the coating process, the wafer holder was rotated continuously at 30 rpm to ensure layer uniformity. Deposition rates and film thickness were controlled in real time using quartz crystal monitoring. Transmission electron microscopy (TEM) was used to confirm the film thicknesses. Prior to deposition of the Gd layer, the oxygen content in the vacuum chamber was minimized by predepositing the Gd metal while keeping the shutter closed. This further decreases the pressure by absorbing the residual oxygen molecules in the vacuum chamber. Following the deposition of silica and Gd metal layers, the wafer substrates were sonicated in a toluene suspension to etch away the polymer beads, leaving the Gd@SiO_2 nanostructures freely suspended in solution. The nanostructures were then collected by multiple centrifugation steps and suspended in ethanol for future use.

The morphology of the nanostructures was imaged using SEM (JEOL JSM 7500F) and TEM (FEI CM120). High-resolution TEM (HRTEM, FEI Titan S/TEM) operated at 300 kV was used to image the nanolayer compositions. The crystal structures were characterized from powder samples using an X-ray diffractometer (XRD, Bruker D8 Discover Powder X-ray Diffractometer). The HRTEM samples were prepared using a FEI Nova 600 dual-beam SEM/FIB (scanning electron microscope/focused ion beam) system. Magnetic property measurements were conducted using a Quantum Design MPMS® XL superconducting quantum interference device (SQuID) magnetometer with applied field strengths of up to $\mu_0 H = 5\,\mathrm{T}$. Magnetization measurements at 5 T are referred to as "saturation magnetization" in this paper because although Gd is still not completely saturated at 5 T, previous studies showed that further increases in the applied magnetic field do not lead to a significant increase in the magnetization for the commonly available laboratory field strengths. The magnetization data were corrected for the diamagnetic response of the sample holder and other background contributions.

III. RESULTS AND DISCUSSION

Figure 1(a) shows an SEM image of the nanoparticles depicting their bowl-shaped structures. The TEM image in Figure 1(b) reveals the core-shell type structure of the particles where the light gray layer corresponds to the capping SiO_2 layer and the darker shades represent the Gd layer located in the core of the nanoconstruct (middle layer). The inset in Figure 1(b) shows the Gd and SiO_2 layers. The Gd layer was polycrystalline whereas no crystallinity was observed for the silica layer. Both SEM and TEM images confirmed the narrow size distribution of the nanoparticles, which is a direct consequence of the controllable nanofabrication approach employed here.

Crystal structure analysis was done at room temperature using Θ–2Θ scans. The shape and width of the XRD spectra peaks were determined using the Rietveld refinement technique. The XRD patterns in Fig. 2(a) reveal that all samples are polycrystalline. A peak analysis reveals the predominance of the hcp (hexagonal close-packed) phase of Gd in the samples (JCPDS: 65-0372). A second, smaller, metastable face-centered cubic (fcc), Gd phase (JCPDS: 65-8099) was also observed with $a = (5.35 \pm 0.02)$ Å. Such an fcc phase for Gd was also reported previously[1,12,13,19,22,25,26] for the case of Gd thin films, nanoparticles, and nanostructures. The fcc peaks were observed at $2\theta = 28.6°$ and $2\theta = 33.2°$,

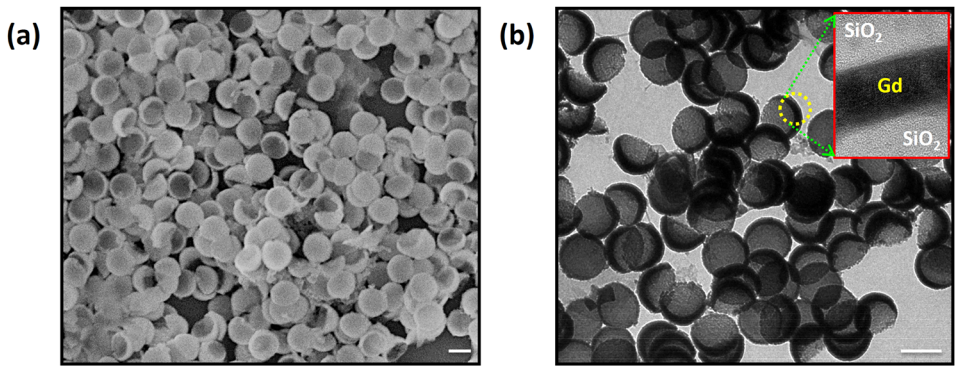

FIG. 1. (a) SEM and (b) TEM images of the nanobowls. Scale bars, 100 nm. The inset image in (b) shows the Gd core and silica shell layers as obtained from HRTEM measurements.

referring to (111) and (200) planes, respectively. The highest intensity peak is associated with the hcp (101) orientation at $2\theta = 32.3°$. We also note that there are no detectable reflections originating from oxide or hydride phases, indicating that the Gd nanoparticles are stable as a result of the protective silica shell coating.

During the coating process, a deposition rate (r) of r = 0.2 Å/s was used for the Gd layer (green spectrum in Figure 2). This sample contains both hcp and fcc phases. When the Gd deposition rate was increased to r = 0.5 Å/s (blue spectrum), the fcc peak intensities for both (111) and (200) were diminished compared to the r = 0.2 Å/s case (Figures 2(b) and 2(c)) whereas the hcp peaks remained unaffected. Therefore, the deposition rate affects the crystallinity of the samples. By controlling the deposition rate, different crystalline compositions could be formed. Scheunert *et al.*,[25] who studied hcp phase formation in thin films, found up to 2% hcp phase content and identified lattice size distortion and strain as being modulated by the deposition conditions.

Figure 3(a) shows the magnetization measurements for samples prepared using different Gd deposition rates. For the sample with r = 0.2 Å/s, the saturation magnetization (M_s) was 203.4 emu/g, whereas it jumped up to 217.5 emu/g for r = 0.5 Å/s. The latter is associated with a fcc content (see Figure 2) significantly lower than the r = 0.2 Å/s sample. The majority of earlier reports[12,19,22] on the magnetic properties of the Gd fcc phase found the fcc phase to be paramagnetic compared to the ferromagnetic hcp phase. However, Bertelli *et al.* recently reported[27] that a ferromagnetic fcc phase could exist for 10 nm-think Gd thin films buffered with a Ta layer. The magnetization of this fcc phase (~175 emu/cm^3 at 60 K) was found to be lower than that of the hcp phase (~640 emu/cm^3 at 60 K). This suggests that magnetization in nanoparticles could be increased by growing particles with minimal fcc and maximal hcp contents.

To investigate the possibility of optimization, we prepared samples with varying Gd deposition rates of r = 0.2 Å/s, 0.5 Å/s, 1 Å/s, 1.5 Å/s, 3 Å/s, and 5 Å/s. As the deposition rate increased from 0.2 Å/s to 1 Å/s, we observed a steady increase in M_s. However, this trend is reversed beyond r = 1 Å/s, where M_s begins to decrease, reaching 208.9 emu/g for r = 5 Å/s (Figure 3(a)). A saturation value of 226.4 emu/g was achieved at r = 1 Å/s, which displayed no detectable presence of fcc phase (see XRD measurements, Figures 2(a)–2(c)). Figures 2(b) and 2(c) show that the (111) and (200) fcc peaks are stronger for r = 0.2 Å/s than they are for r = 3 Å/s, which should result in a higher M_s value for the latter. For these two rates, the M_s values are 203.4 emu/g and 214.7 emu/g, respectively.

The magnetization measurements of Figure 3(a) were recorded for applied fields in the range −5T to 5T. Standard ferromagnetic behavior with hysteresis is observed for all cases even though XRD spectra indicate that some fcc contributions are present in most of the samples. The presence of the ferromagnetic hcp phase in all our samples is consistent

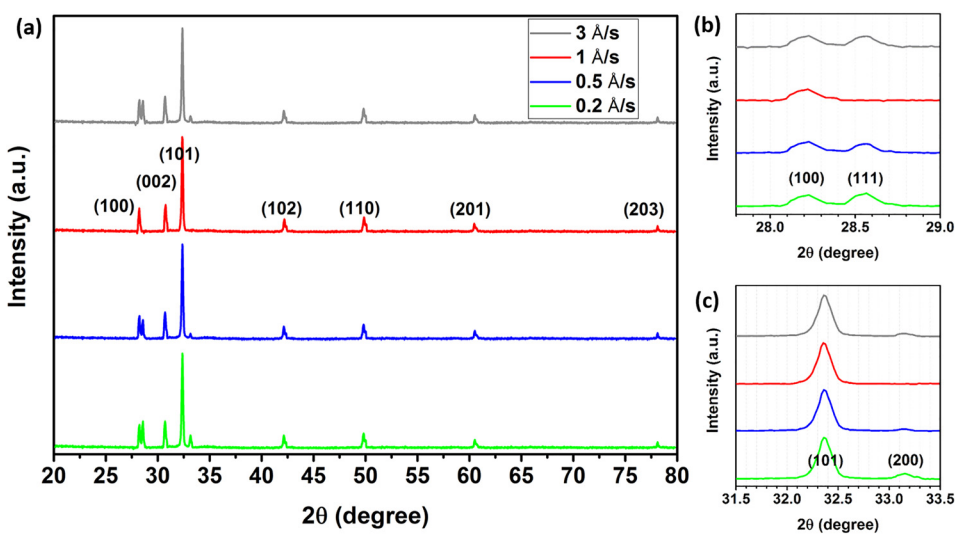

FIG. 2. (a) XRD spectra of the Gd nanoparticles for varying Gd deposition rates (r) of 0.2 Å/s, 0.5 Å/s, 1 Å/s, and 3 Å/s, (b) XRD spectra for $27.8° < 2\theta < 29.0°$, and (c) XRD spectra for $31.5° < 2\theta < 33.5°$.

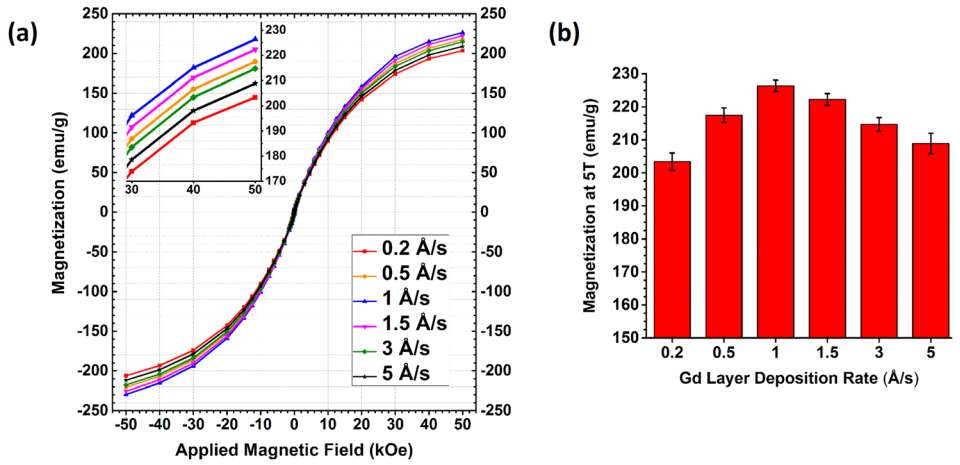

FIG. 3. (a) Magnetization measurements for different Gd deposition rates. Field-dependent magnetization curves indicate a trend towards saturation in magnetization at high magnetic fields (5 T). The top left inset shows that saturation magnetization peaks at deposition rate = 1 Å/s, reaching 226.4 emu/g whereas it dips at deposition rate = 0.2 Å/s, decreasing to 203.4 emu/g. The bottom left inset reveals hysteresis associated with ferromagnetism. (b) Saturation magnetization versus deposition rate of the Gd layer. Error bars indicate the variation of M_s obtained from 5 separate runs for each set of deposition parameters. M_s peaks at 1 Å/s, reaching 226.4 emu/g, and decays as the rate goes further on both sides of 1 Å/s.

with the observation of magnetic hysteresis. The presence of a small amount of the paramagnetic fcc phase in the samples is reflected in the magnetic measurements as far as its effect is to decrease the saturation magnetization (Fig. 3). The saturation magnetization of the fcc phase of Gd has been shown to be approximately 4 times less than that of hcp Gd ($\sim$175 emu/cm^3 vs. $\sim$640 emu/cm^3 at 60 K) according to Bertelli *et al.*[27] From the XRD data, we compute *s*, the ratio between the area under the strongest Bragg peaks of the hcp (101) and fcc (200) phases, defined as $s = A_{fcc}/A_{hcp}$ (%). For the sample with lowest magnetization (r = 0.2 Å/s), *s* was found to be 12.2%, whereas for the optimal condition (highest M_s, r = 1 Å/s), *s* approaches zero as the fcc peaks were no longer detectable, buried in the noise. These results are shown in Table II for different deposition rates. We note the inverse correlation between *s* and M_s. We calculate the expected value of M_s values based on the measured M_s value for fcc Gd (Ref. 24) as a weighted average of fcc and hcp fractions (1)

$$\text{expected } M_s = (226.4)(1-s) + \left(\frac{226.4}{4}\right)(s), \qquad (1)$$

where *s* is a number between 0 and 1 (expressed as a percentage) and $\frac{226.4}{4}$ is the M_s value for fcc Gd from Ref. 27. The expected values of M_s are close to the observed values. Thus, we conclude that the observed decreases in saturation magnetization values at different deposition rates can be accounted for by the less magnetic fcc fraction.

TABLE II. Crystalline phase composition and corresponding magnetization values for Gd nanobowls fabricated using different Gd deposition rates.

Gd deposition rate (Å/s)	Area fcc (a.u.)	Area hcp (a.u.)	s factor (%)	Expected M_s (emu/g)	Observed M_s (emu/g)
0.2	57.4	469.1	12.2%	205.7	203.4
0.5	19.2	468.7	4.1%	219.4	217.5
1	$\sim$0	469.4	$\sim$0%	226.4	226.4
3	30.8	471.7	6.5%	215.4	214.7

To check that the observed changes in M_s are not due to random errors or other effects, error bars were obtained by repeating the experiments on different days using the same nominal parameters. Figure 3(b) shows the saturation magnetization values for different Gd deposition rates and the corresponding error bars for each case, which represent 5 different measurements. It is seen that the statistical fluctuations in magnetization values (for example, $M_s = 226.4 \pm 1.7$ emu/g for r = 1 Å/s) are lower than the observed changes in M_s. Thus, random errors do not account for the observed trends in Figure 3(b). We conclude that the deposition rate has a direct effect on the observed magnetization values.

The lowest saturation magnetization value was found at the lowest deposition rate (r = 0.2 Å/s), where the highest content of the fcc phase was measured. The presence of the fcc phase could lead to a significant contribution of intergrain and intragrain anisotropies.[1] The highest saturation magnetization we obtained was 226.4 emu/g (at 2 K), which is lower than the theoretical maximum (268 emu/g) but higher than any other Gd nanoparticles produced to date. The difference from the bulk value may be due to interfacial effects[22,23] present in nanostructures. There have been several reports[1,25] of Gd thin films preferring to nucleate at a seed boundary in a paramagnetic fcc phase. Since the substrate (curved surface of amorphous silica here) affects the growth, other choices of geometries and materials such as Mn, Pd, Cr, or W would be expected to lead to different magnetic properties.[28] The polycrystalline nature[23] of the samples, random grain formations,[10,11,18,23,25] crystal defects,[11] and stress[1,18,25] likely act as barriers in achieving high magnetism by distorting the magnetization uniformity.

IV. CONCLUSION

In summary, we have applied a nanofabrication approach to prepare air stable core-shell Gd nanoparticles with high magnetic moments. Crystallinity of the nanoparticles played

an important role in maximizing magnetization. The ferromagnetic hcp phase of Gd was the main dominant crystal structure whereas small amounts of the paramagnetic fcc phase could be detected. We have experimentally shown that a lower fcc content leads to higher saturation magnetization. We found that by adjusting the deposition rate of Gd, it is possible to control the amount of the fcc content in the lattice. A deposition rate of 1 Å/s led to the highest magnetic moment of 226.4 emu/g for Gd. Such a high magnetization has never been observed experimentally to date for Gd nanoparticles. Stability of the nanoparticles along with their high magnetizations could give rise to new applications for Gd, which have not been possible so far due to oxidation problems in ambient air.

ACKNOWLEDGMENTS

L.-S. B. acknowledges funding from the Arnold and Mabel Beckmann Foundation (Young Investigator Award). We acknowledge the use of nanofabrication equipment in the ISNC Cleanroom facility and electron microscopy in the EICN facility of the California NanoSystems Institute (CNSI), in particular, Dr. Ivo Atanasov for assistance with HRTEM imaging.

[1]G. Scheunert, W. R. Hendren, C. Ward, and R. M. Bowman, Appl. Phys. Lett. **101**, 142407 (2012).
[2]M. Chakravorty and A. K. Raychaudhuri, J. Appl. Phys. **115**, 054308 (2014).
[3]M. A. Ruderman and C. Kittel, Phys. Rev. **96**, 99 (1954).
[4]K. A. Gschneidner, V. K. Pecharsky, and A. O. Tsokol, Rep. Prog. Phys. **68**, 1479 (2005).
[5]D. C. F. Soares, M. A. de Barros Correia Menezes, R. G. dos Santos, and G. A. Ramaldes, J. Radioanal. Nucl. Chem. **284**, 315 (2010).
[6]S. M. Borisov and I. Klimant, Anal. Bioanal. Chem. **404**, 2797 (2012).
[7]Y. N. Ertas, N. N. Jarenwattananon, and L. S. Bouchard, Chem. Mater. **27**, 5371 (2015).
[8]U. Stetter, M. Farle, K. Baberschke, and W. G. Clark, Phys. Rev. B **45**, 503 (1992).
[9]J. S. Jiang and C. L. Chien, J. Appl. Phys. **79**, 5615 (1996).
[10]M. Yue, J. X. Zhang, H. Zeng, and K. Wang, Appl. Phys. Lett. **89**, 232504 (2006).
[11]F. Döbrich, M. Elmas, A. Ferdinand, J. Markmann, M. Sharp, H. Eckerlebe, J. Kohlbrecher, R. Birringer, and A. Michels, J. Phys.: Condens. Matter **21**, 156003 (2009).
[12]X. G. Liu, D. Y. Geng, Q. Zhang, J. J. Jiang, W. Liu, and Z. D. Zhang, Appl. Phys. Lett. **94**, 103104 (2009).
[13]I. Aruna, B. R. Mehta, L. K. Malhotra, and S. M. Shivaprasad, Adv. Funct. Mater. **15**, 131 (2005).
[14]M. J. O'Shea and P. Perera, J. Appl. Phys. **85**, 4322 (1999).
[15]J. A. Nelson, L. H. Bennett, and M. J. Wagner, J. Am. Chem. Soc. **124**, 2979 (2002).
[16]Y. Z. Shao, C. H. Shek, and J. K. L. Lai, J. Mater. Res. **13**, 2969 (1998).
[17]P. Z. Sil. Škorvánek, J. Kováč, D. Y. Geng, X. G. Zhao, and Z. D. Zhang, J. Appl. Phys. **94**, 6779 (2003).
[18]Z. C. Yan, Y. H. Huang, Y. Zhang, H. Okumura, J. Q. Xiao, S. Stoyanov, V. Skumryev, G. C. Hadjipanayis, and C. Nelson, Phys. Rev. B **67**, 054403 (2003).
[19]C. J. Hsu, S. V. Prikhodko, C. Y. Wang, L. J. Chen, and G. P. Carman, J. Appl. Phys. **111**, 053916 (2012).
[20]H. E. Nigh, S. Legwold, and F. H. Spedding, Phys. Rev. **132**, 1092 (1963).
[21]C. Yan and M. Wagner, Nano Lett. **13**, 2611 (2013).
[22]C. Ward, G. Scheunert, W. R. Hendren, R. Hardeman, M. A. Gubbins, and R. M. Bowman, Appl. Phys. Lett. **102**, 092403 (2013).
[23]S. P. Mathew and S. N. Kaul, J. Phys.: Condens. Matter **24**, 256008 (2012).
[24]M. Chakravorty and A. K. Raychaudhuri, J. Appl. Phys. **117**, 034301 (2015).
[25]G. Scheunert, C. Ward, W. R. Hendren, A. A. Lapicki, R. Hardeman, M. Mooney, M. Gubbins, and R. M. Bowman, J. Phys. D: Appl. Phys. **47**, 415005 (2014).
[26]A. E. Curzon and H. G. Chlebek, J. Phys. F: Metal Phys. **3**, 1 (1973).
[27]T. P. Bertelli, E. C. Passamani, C. Larica1, V. P. Nascimento, A. Y. Takeuchi, and M. S. Pessoa, J. Appl. Phys. **117**, 203904 (2015).
[28]G. Scheunert, O. Heinonen, R. Hardeman, A. Lapicki, M. Gubbins, and R. M. Bowman, Appl. Phys. Rev. **3**, 011301 (2016).